The Effect of Partial Coherence In Receiving System Noise Temperature on Array Gain for Telemetry and Radio Frequency Carrier Reception for Receiving Systems with Unequal Predetection Signal-to-Noise Ratios

M. H. Brockman
Telecommunications Science and Engineering Division

Signal-to-noise ratio improvement realized by arraying receiving systems or stations for coherent reception is reduced when some portion of the predetection noise is coherent in the array. This article examines this effect for arrayed receiving systems with unequal apertures including expected performance for selected planets of the solar system within the array beamwidth.

I. Introduction

An earlier report (Ref. 1) considered the effect of partial coherence in system noise temperature on predetection signal-to-noise ratio improvement and equivalent radio frequency (RF) carrier signal-to-noise ratio improvement for coherent reception and demodulation for an array of similar receiving systems with essentially equal predetection noise and equal size antenna apertures. This report examines the effect of partial coherence in system noise temperature on predetection signal-to-noise ratio improvement and RF carrier margin improvement for coherent reception and demodulation for an array of receiving systems with unequal predetection noise and unequal antenna apertures. The analytic expressions given represent the general case for the configuration examined here.

Performance is presented in this report for the case which is representative of 34-meter-diameter antenna receiving systems arrayed with a 64-meter-diameter antenna receiving system which also has transmit capability. For the performance shown here, the coherent portion of predetection noise (which is coherent periodically) results from a planet in the solar system which is within the beamwidth of the antennas of the array. RF carrier array gain measurements made in the Laboratory for simulated 64-meter/34-meter antenna receiving system arrays are compared with theoretical results.

This report also provides information on the expected periodic reduction in array gain at a reception frequency of 8420 MHz due to antenna feed spacing with the planets Jupiter or Venus in the array beamwidth. The expected periodic reduction in array gain with these planets in the array beamwidth is less than 0.2 dB for a two-aperture array and less than 0.25 dB for a three-aperture array for the antenna spacings and orientation planned for the 64- and 34-meter antennas at the three DSN complexes. Expected reduction in array gain with the planets Uranus or Neptune in the array beamwidth is negligible.

II. Predetection Signal-to-Noise Ratio and Resultant Carrier Tracking Loop Phase Noise

Figure 1 illustrates the configuration considered herein which provides predetection signal-to-noise ratio improvement and equivalent RF carrier signal-to-noise ratio improvement (RF carrier margin improvement) for high rate telemetry with residual RF carrier. The RF carrier margin improvement also provides a corresponding improvement in minimum RF carrier level for radio metric tracking. Figure 1 and a modification of Fig. 1 (so that much larger antenna separations for the array can be handled conveniently) were presented in Ref. 1 with a discussion of predetection noise resulting from operating equivalent system noise temperature T_{op}.

With receiving system 2 connected to the summing junction (see Fig. 1), the RF carrier predetection signal-to-noise ratio in receiving system 1 at the output of the summing junction is (from Expression 3, Ref. 1):

$$\frac{P_{c1_{\Sigma 1.2}}}{P_{n1_{\Sigma 1.2}}} = \frac{(A_1 \cos m_{pd} + \beta_2 A_2 \cos m_{pd})^2}{\left[NBW_{F_{A1}} (1-\epsilon_1) N_{o1} + \beta_2^2 NBW_{F_{A2}} (1-\epsilon_2) N_{o2}\right] + \left[(NBW_{F_{A1}} \cdot \epsilon_1 N_{o1})^{1/2} + \beta_2 NBW_{F_{A2}} \cdot \epsilon_2 N_{o2})^{1/2}\right]^2} \tag{1}$$

where $NBW_{F_{A1}}$ represents the noise bandwidth of second IF filter F_{A1}, $NBW_{F_{A2}}$ is equal to $NBW_{F_{A1}}$, N_{o1} is the one-sided noise spectral density for receiving system 1 related to T_{op1}, and N_{o2} is the noise spectral density of receiving system 2 related to T_{op2}. The term β_2 is the voltage coupling of receiving system 2 relative to receiving system 1 at the summing junction, and γ_2^2 is the carrier power-to-noise spectral density ratio of receiving system 2 relative to receiving system 1. The statistically independent portion of predetection noise is $(1 - \epsilon_1)$ in receiving system 1 and $(1 - \epsilon_2)$ in receiving system 2. The corresponding portion of predetection noise that is coherent is ϵ_1 and ϵ_2 in the two receiving systems. Expression 1 can be rewritten as

$$\frac{P_{c1_{\Sigma 1.2}}}{P_{n1_{\Sigma 1.2}}} = \frac{P_{c1}}{NBW_{F_{A1}} \cdot N_{o1}} \cdot \frac{(1+\beta_2\gamma_2)^2}{\left[(1-\epsilon_1) + (1-\epsilon_2)\frac{N_{o2}}{N_{o1}}\beta_2^2\right] + \left[\epsilon_1^{1/2} + \epsilon_2^{1/2}\left(\frac{N_{o2}}{N_{o1}}\right)^{1/2}\beta_2\right]^2} \tag{2}$$

Note that (from Ref. 1) the predetection carrier signal-to-noise ratio in receiving system 1 (with receiving system 2 switched out of the summing junction) is $P_{c1}/(NBW_{F_{A1}} \cdot N_{o1})$. Consequently, the improvement in predetection signal-to-noise ratio for two receiving systems arrayed (n_2'') is:

$$n_2'' = \frac{(1+\beta_2\gamma_2)^2}{\left[(1-\epsilon_1) + (1-\epsilon_2)\frac{N_{o2}}{N_{o1}}\beta_2^2\right] + \left[\epsilon_1^{1/2} + \epsilon_2^{1/2}\left(\frac{N_{o2}}{N_{o1}}\right)^{1/2}\beta_2\right]^2} \tag{3}$$

For N receiving systems arrayed, the predetection carrier signal-to-noise ratio in receiving system 1 becomes

$$\frac{P_{c1\Sigma 1,\cdots,N}}{P_{n1\Sigma 1,\cdots,N}} = \frac{P_{c1}}{NBW_{F_{A1}} \cdot N_{o1}} \cdot \frac{(1+\beta_2\gamma_2+\cdots\beta_N\gamma_N)^2}{\left[(1-\epsilon_1)+(1-\epsilon_2)\frac{N_{o2}}{N_{o1}}\beta_2^2+\cdots+(1-\epsilon_N)\frac{N_{oN}}{N_{o1}}\beta_N^2\right]+\left[\epsilon_1^{1/2}+\epsilon_2^{1/2}\left(\frac{N_{o2}}{N_{o1}}\right)^{1/2}\beta_2+\cdots+\epsilon_N^{1/2}\left(\frac{N_{oN}}{N_{o1}}\right)^{1/2}\beta_N\right]^2} \tag{4}$$

The improvement in predetection signal-to-noise ratio for N receiving systems arrayed is then

$$n_N'' = \frac{(1+\beta_2\gamma_2+\cdots\beta_N\gamma_N)^2}{\left[(1-\epsilon_1)+(1-\epsilon_2)\frac{N_{o2}}{N_{o1}}\beta_2^2+\cdots+(1-\epsilon_N)\frac{N_{oN}}{N_{o1}}\beta_N^2\right]+\left[\epsilon_1^{1/2}+\epsilon_2^{1/2}\left(\frac{N_{o2}}{N_{o1}}\right)^{1/2}\beta_2+\cdots+\epsilon_N^{1/2}\left(\frac{N_{oN}}{N_{o1}}\right)^{1/2}\beta_N\right]^2} \tag{5}$$

It should be noted (as discussed in Ref. 1) that for the condition where the varying group delay on the telemetry sidebands is tracked out among the various receiving systems of the array (which is accomplished at baseband for the configuration shown in Fig. 1), the improvement in telemetry predetection signal-to-noise ratio that can be obtained is also represented by expressions (3) and (5) for the corresponding voltage coupling β in the signal spectrum combining process and ratio of signal-to-noise spectral density ratios γ^2 for telemetry. However, the predetection signal-to-noise ratio improvement obtained for telemetry does not include loss in the telemetry signal spectrum combining process and the loss (radio loss) due to carrier tracking loop phase noise.

The resultant rms phase noise ($\sigma_{\Phi_{n1\Sigma 1,2}}$) at the output of the RF carrier tracking loop (i.e., on the first local oscillator signal) in receiving system 1 due to the predetection signal-to-noise ratio within the closed-loop noise bandwidth of the RF carrier tracking loop becomes (see expression 7, Ref. 1)

$$\sigma_{\phi_{n1\Sigma 1,2}} = \frac{\frac{N_{o1}}{2}\cdot 2B_{L1}}{P_{c1}} \cdot \frac{1}{n_2''}\left[\frac{1+\frac{P_{c1}\,n_2''}{NBW_{F_{A1}}\cdot N_{o1}}}{0.862+\frac{P_{c1}\cdot\eta_2''}{NBW_{F_{A1}}\cdot N_{o1}}} \cdot \frac{\exp\left(\frac{N_{o1}\cdot B_{L1}}{P_{c1}\cdot\eta_2''}\right)}{\sinh\left(\frac{N_{o1}\cdot B_{L1}}{P_{c1}\cdot\eta_2''}\right)}\right]^{1/2} \text{rad, rms} \tag{6}$$

for two systems arrayed where n_2'' is defined in expression (3) above. For N receiving systems arrayed, the resultant rms phase noise ($\sigma_{\phi_{n1\Sigma 1,\cdots,N}}$) becomes

$$\sigma_{\phi_{n1\Sigma 1,\cdots,N}} = \frac{\frac{N_{o_N}}{2}\cdot B_{L1}}{P_{c1}} \cdot \frac{1}{n_N''}\left[\frac{1+\frac{P_{c1}\cdot n_N''}{NBW_{F_{A1}}\cdot N_{o1}}}{0.862+\frac{P_{c1}\cdot n_N''}{NBW_{F_{A1}}\cdot N_{o1}}} \cdot \frac{\exp\left(\frac{N_{o1}\cdot B_{L1}}{P_{c1}\cdot n_N''}\right)}{\sinh\left(\frac{N_{o1}\cdot B_{L1}}{P_{c1}\cdot n_N''}\right)}\right]^{1/2} \text{rad, rms} \tag{7}$$

where n_N'' is defined in expression (5) above. The rms phase noise $\sigma_{\phi_{n1}}$ for receiving system 1 with receiving systems 2 through N switched out of the summing junction is shown in Ref. 1 (expression 2).

Note that the total phase noise at the output of the principal carrier tracking loop (i.e., on the first local oscillator) becomes

$$\left[\sigma^2_{\phi_{n1\Sigma 1,2}} + \left(\frac{\beta_2 \sigma_{\phi_{n2}}}{1+\beta_2}\right)^2\right]^{1/2} \tag{8}$$

for two receiving systems arrayed (see Ref. 1). For N receiving systems arrayed, the total rms phase noise on the first local oscillator is

$$\left[\sigma^2_{\phi_{n1\Sigma 1,\cdots,N}} + \left(\frac{\beta_2 \sigma_{\phi_{n2}}}{1+\beta_2}\right)^2 + \cdots + \left(\frac{\beta_N \sigma_{\phi_{nN}}}{1+\beta_N}\right)^2\right]^{1/2} \tag{9}$$

Expressions for rms phase noise in systems 2 through N were developed in Ref. 1.

As developed in Ref. 1, the total rms phase noise in expressions (8) and (9) can be considered as due to an equivalent carrier predetection signal-to-noise ratio within the closed-loop noise bandwidth of the RF carrier phase tracking loop. Comparison of this equivalent carrier signal-to-noise ratio with the initial carrier predetection signal-to-noise ratio in a single receiving system (i.e., system 1) alone provides the improvement in carrier margin due to radio frequency carrier arraying for the high rate telemetry configuration where some portion of the predetection noise is not statistically independent among the various receiving systems of the array.

III. Performance

Expressions (3) and (5) represent improvement in predetection signal-to-noise ratio in receiving system 1 under the condition that the phase shift and group delay in the various receiving systems of the array are essentially matched in a predetection bandwidth that encompasses the signal of interest. In addition for telemetry (as described in Ref. 1), expressions (3) and (5) apply for the additional condition that the varying group delay on the signal modulation sidebands is tracked out among the receiving systems of the array by a telemetry signal spectrum combiner during a station pass. Note again that the predetection signal-to-noise ratio improvement for telemetry does not include the telemetry signal combiner loss and the loss (radio loss) due to carrier tracking loop phase noise. Reference 2 provides information on radio loss.

Improvement in receiving system 1 predetection signal-to-noise ratio is shown in Fig. 2 as a function of the statistically independent (noncoherent) portion of predetection noise $(1 - \epsilon_1)$ in receiving system 1 for an array consisting of a 64-meter-diameter antenna with a 50% aperture efficiency (system 1) and a 34-meter-diameter antenna listen-only, with a 60% aperture efficiency. As pointed out in Section I, for the performance shown in this report, the coherent portion of predetection noise results from a planet in the solar system which is within the beamwidth of the antennas of the array. Consequently, the coherent noise for the 34-meter-diameter listen antenna is scaled relative to the 64-meter-diameter antenna by $(34/64)^2 \times (0.60/0.50)$. Performance is shown for γ_2 values of 0.55, 0.61, and 0.66 for the case where $\beta_2 = \gamma_2$. As developed earlier in this report, γ_2^2 is the signal-power-to-noise-spectral-density ratio of receiving system 2 relative to the receiving system 1, and β_2 is the voltage coupling of receiving system 2 relative to receiving system 1 for the combining process. Improvement in predetection signal-to-noise ratio is maximum for $\beta = \gamma$ when the predetection noise is all statistically independent or $1 - \epsilon_1 = 1$, which is representative for the DSN most of the time. A γ_2 value of 0.61 represents the nominal value for this array and provides a 1.46-dB improvement in predetection signal-to-noise ratio at $\beta = \gamma$ for $1 - \epsilon_1 = 1$. A γ_2 value of 0.66 represents operation of the antennas at low (10-15 deg) and high (approximately 80 deg) elevation angles, whereas a γ_2 value of 0.55 represents a below nominal signal-to-noise ratio for the 34-m antenna (listen-only). The ratio of noise spectral densities (N_{o2}/N_{o1}) used in Fig. 2 for noncoherent predetection noise $(1 - \epsilon_1 = 1)$ is 0.925 (18.5K/20.0K). A N_{o2}/N_{o1} value of 1 for $1 - \epsilon_1 = 1$ reduces the improvement in predetection signal-to-noise ratio shown in Fig. 2 by about 0.1 dB and less than 0.1 dB for $1 - \epsilon_1$ less than 1.[1] The resultant decrease in predetection signal-to-noise ratio improvement is shown in Fig. 2 as an increasing portion of predetection noise becomes coherent

[1] A N_{o2}/N_{o1} of 0.925 (18.5/20.0) represents operation at high elevation angles, while at low elevation angles, N_{o2}/N_{o1} approaches a value of 1.

(ϵ_1) or as the statistically independent portion of predetection noise ($1 - \epsilon_1$) decrease for receiving system 1. An increase in aperture efficiency for the 34-meter-diameter listen antenna to 65% reduces the improvement in predetection signal-to-noise ratio shown in Fig. 2 by about 0.1 dB at $1 - \epsilon_1 = 0.3$ and has no effect when $1 - \epsilon_1 = 1$ for a given γ_2 value.

Figure 3 shows receiving system 1 predetection signal-to-noise ratio improvement as a function of the statistically independent portion of system 1 predetection noise ($1 - \epsilon_1$) for an array of two receiving systems utilizing a 64-meter-diameter antenna and a 34-meter-diameter antenna (transmit/receive) (with a 54% aperture efficiency), for γ_2 values of 0.48, 0.53, and 0.58. Coherent noise for the 34-meter-diameter transmit/receive antenna is scaled relative to the 64-meter-diameter antenna by $(34/64)^2 \times (0.54/0.50)$. A nominal γ_2 value of 0.53 provides a 1.0-dB improvement in predetection signal-to-noise ratio for $1 - \epsilon_1 = 1$. The preceding discussion for γ_2 values of 0.55, 0.61, and 0.66 for Fig. 2 applies to the γ_2 values of 0.48, 0.53, and 0.58 respectively for Fig. 3. The ratio of noise spectral densities (N_{o2}/N_{o1}) is 1.075 (21.5K/20.0K) for noncoherent predetection noise ($1 - \epsilon_1 = 1$) in Fig. 3. In this case, a N_{o2}/N_{o1} value of 1 for $1 - \epsilon_1 = 1$ increases the improvement in predetection signal-to-noise ratio shown in Fig. 3 by 0.1 dB (or less). A decrease in aperture efficiency for the 34-meter-diameter transmit/receive antenna to 50% increases the improvement in predetection signal-to-noise ratio shown in Fig. 3 by about 0.1 dB at $1 - \epsilon_1 = 0.3$ and has no effect when $1 - \epsilon_1 = 1$ for a given γ_2 value.

Figures 4 and 5 show improvement in receiving system 1 predetection signal-to-noise ratio for an array of three receiving systems as a function of the statistical independent portion of predetection noise ($1 - \epsilon_1$) in receiving system 1 for the case where $\beta_2 = \beta_3 = \gamma_2$. Figure 4 represents an array utilizing a 64-meter-diameter antenna (system 1), a 34-meter-diameter antenna listen-only (system 2) and a 34-meter-diameter antenna with transmit/receive capability (system 3). Nominal values of $\gamma_2 = 0.61$ and $\gamma_3 = 0.53$ provide a 2.17-dB improvement in predetection signal-to-noise ratio for $1 - \epsilon_1 = 1$ (Fig. 4). For this figure, the ratio of noise spectral densities N_{o2}/N_{o1} and N_{o3}/N_{o1} are 0.925 and 1.075 respectively at $1 - \epsilon_1 = 1$. A value of 1 for N_{o2}/N_{o1} and N_{o3}/N_{o1} provides essentially the same performance as shown in Fig. 4. Figure 4 represents performance for aperture efficiencies of 50, 60, and 54% for receiving systems 1, 2, and 3 respectively for the three sets of values for γ_2 and γ_3 shown in Fig. 4. An increase in aperture efficiency to 65% for the 34-meter-diameter listen antenna and a decrease in aperture efficiency to 50% for the 34-meter-diameter transmit/receive antenna reduce the improvement in predetection signal-to-noise ratio shown in Fig. 4 by about 0.05 dB at $1 - \epsilon_1 = 0.3$ and has no effect when $1 - \epsilon_1 = 1$ for a given set of γ_2 and γ_3 values. Figure 5 represents an array utilizing a 64-meter-diameter antenna (system 1) and two 34-meter-diameter antennas listen-only (systems 2 and 3) with 60% aperture efficiencies. Nominal values of $\gamma_2 = \gamma_3 = 0.61$ provide a 2.55-dB improvement in predetection signal-to-noise ratio for $1 - \epsilon_1 = 1$ and $N_{o2}/N_{o1} = N_{o3}/N_{o1} = 0.925$. A value for 1 for N_{o2}/N_{o1} and N_{o3}/N_{o1} decreases the improvement in predetection signal-to-noise ratio shown in Fig. 5 by 0.15 dB (or less). An increase in aperture efficiency to 65% for systems 2 and 3 reduces the predetection signal-to-noise ratio improvement shown in Fig. 5 by about 0.2 dB at $1 - \epsilon_1 = 0.3$ and has no effect when $1 - \epsilon_1 = 1$ for a given set of γ_2 and γ_3 values.

Figures 6, 7, 8, and 9 show the effect on predetection signal-to-noise ratio improvement as the voltage coupling β in the signal combining or summing process is varied for two and three receiving systems arrayed. The array parameters for Figs. 6, 7, 8, and 9 are as described above for Figs. 2, 3, 4, and 5 respectively. Also shown in Figs. 6, 7, 8, and 9 is the effect of predetection signal-to-noise ratio improvement when the portion of predetection noise that is statistically independent ($1 - \epsilon_1$) is 1.0, 0.7, or 0.3 in receiving system 1.

Consider next the equivalent RF carrier predetection signal-to-noise ratio improvement (RF carrier margin improvement) as determined from the total rms phase noise on the first local oscillator (see expressions (6), (7), (8), and (9) and associated discussion in Section II). The following sets of design parameters apply for the performance presented in this report. The sets of parameters for receiving system 1 are:

Threshold two-sided noise bandwidth $2B_{L_{o1}}$	12	152	30 Hz
Predetection IF filter noise bandwidth $NBW_{F_{A1}}$	2200	2200	2000 Hz

while the corresponding sets of parameters for receiving system 2 through N are:

Threshold two-sided noise bandwidth $2B_{L_{o2,\cdots,N}}$	0.1	1.0	0.3 Hz
Predetection IF filter noise bandwidth $NBW_{F_{A2,\cdots,N}}$	2200	2200	2000 Hz

Using the bandwidth parameters above and the array parameters described in conjunction with Fig. 2, Fig. 10 shows the RF carrier margin improvement as a function of summing junction voltage coupling β. Figure 10 represents an array of two receiving systems with a 64-meter-diameter antenna (system 1) and a 34-meter-diameter antenna listen-only (system 2). Performance is shown for γ_2 values of 0.55, 0.61, and 0.66 with $1 - \epsilon_1$ values of 1.0, 0.7, and 0.3 as in Fig. 6. The information in Fig. 10 can be rearranged to show RF carrier margin improvement as a function of the statistically independent portion of predetection noise in system 1 ($1 - \epsilon_1$). Figure 11 shows this characteristic for a voltage coupling $\beta_2 = \gamma_2$ for γ_2 values of 0.55, 0.61, and 0.66.

Figures 12 and 13 show similar RF carrier margin improvement characteristics for an array of two receiving systems with a 64-meter-diameter antenna and a 34-meter-diameter antenna, transmit/receive. Similar characteristics are shown in Figure 14 and 15 for an array of three receiving systems with a 64-meter-diameter antenna (system 1), a 34-meter-diameter antenna listen-only (system 2) and a 34-meter-diameter antenna (transmit/receive) (system 3). Figures 16 and 17 show RF carrier margin improvement characteristics for an array of three receiving systems with a 64-meter-diameter antenna (system 1) and two 34-meter-diameter antenna (listen-only).

Some initial measurements of RF carrier margin improvement have been made in the laboratory, for two and three receiving systems arrayed, by measurement of rms phase noise (σ_{ϕ_n}) on the first local oscillator signal in system 1 and utilizing this σ_{ϕ_n} in conjunction with expressions (6) and (7) in Section II. For these measurements, γ_2 and γ_3 values of 0.61 were set up in the laboratory to simulate reception with 34-meter-diameter antenna(s) (listen-only) arrayed with a 64-meter-diameter antenna (system 1). Measurements were made using the following set of parameters. The predetection IF filter noise bandwidth was 2200 Hz with a $2B_{L_o}$ of 152 Hz for receiving system 1 and $2B_{L_o}$ of 1 Hz for receiving systems 2 and 3.

The statistically independent noise ($1 - \epsilon$) coupled into the input of each receiving system from separate random noise sources was equal so that $N_{o2}/N_{o1} = N_{o3}/N_{o1} = 1$ for $1 - \epsilon_1 = 1$. Coherent noise (ϵ) coupled into the input of the simulated 34-meter receiving systems was scaled by the ratio $(34/64)^2 \times (0.6/0.5)$ relative to the simulated 64-meter receiving system and adjusted for correlation. The values 0.6 and 0.5 represent the aperture efficiencies, discussed earlier, of the 34-meter-diameter antenna listen-only and the 64-meter-diameter antenna respectively. Table 1 shows the experimental measurements relative to the calculated results.

IV. Discussion

The situation where a planet in the solar system is within the beamwidth of an array with equal antenna apertures was examined in Ref. 1 (Section V). The receiving systems were arrayed for coherent reception of a signal from a spacecraft in deep space. The same situation is considered herein except that the antennas of the array have unequal apertures as presented in the earlier sections of this report.

Consider the case (as in Ref. 1) of two receiving systems arrayed for coherent reception of the spacecraft signal. A two-aperture (antenna) array will see the hot body (noise) radiation from the planet as an interferometer operating at a reception frequency wavelength λ with an antenna spacing $B_{1,2}$. Designate the component of $B_{1,2}$ that is perpendicular to the line of sight to the planet as $B_{r_{1,2}}$; then the resultant fringe spacing of the interferometer is $\lambda/B_{r_{1,2}}$ radians.

A large part of the following material was presented in Ref. 1 and is included here for clarification and continuity of discussion. Consider for the moment, a situation where the planet appears as a point noise source. That is, the angular size of the planet as seen from Earth is very small compared to the fringe spacing ($\lambda/B_{r_{1,2}}$). Within the fringe spacing (as the Earth rotates), the noise radiation from the planet as seen in the predetection bandwidth of the array is in phase for the two receivers at the center of an angular segment $\lambda/2B_{r_{1,2}}$, orthogonal at each edge of the angular segment, and 180 deg out of phase at the center of the adjacent angular segments $\lambda/2B_{r_{1,2}}$ due to continuing change in path length to the two antennas. This in-phase/out-of-phase situation continues alternately during a station pass as the array tracks the spacecraft and it is superimposed on the statistically independent portion of predetection noise. It should be noted again that the varying group delay on the signal modulation sidebands is tracked out among the receiving systems of the array during a station pass (see Section III, first paragraph). For this situation of a planet appearing as a point noise source and representing a given fractional part (ϵ) of operating equivalent system noise temperature (T_{op}), the decrease in predetection signal-to-noise ratio improvement shown in Figs. 2 and 3 (for the corresponding $(1 - \epsilon)$) corresponds to the in-phase predetection noise condition at the center of an angular segment $\lambda/2B_{r_{1,2}}$. The orthogonal predetection point noise source condition corresponds to a signal-to-noise ratio improvement for $(1 - \epsilon) = 1$, while the 180-deg out-of-phase point noise source condition corresponds to a signal-to-noise ratio improvement with a portion of the point source contributions removed (cancelled). The discussion above also applies to RF carrier margin improvement as shown in Figs. 11 and 13 for two systems arrayed. Cross plots of the performance shown in Figs. 6 and 7 and in Figs. 10 and 12 would provide similar information for other signal summing voltage couplings.

A planet for the solar system may not appear as a point noise source for the array considered here. In fact, it can have an angular size that is larger than the fringe spacing $\lambda/B_{r_{1,2}}$. The following development addresses this consideration. In general, for the application presented in this report, the planets (as viewed from Earth) can be characterized as disks with a uniform brightness distribution D at the reception frequency. The brightness distribution will be a function of the reception frequency. Utilizing information in Ref. 3 and writing the brightness transform as a function of the angular size ν of the planet and the inverse of fringe spacing, the brightness transform R becomes

$$R_{1,2} = \frac{1}{\nu} \int_{-\nu/2}^{+\nu/2} D(\omega) e^{-2\pi i \left(\frac{B_{r_{1,2}}}{\lambda}\right) \times dx} \tag{10}$$

with integration from the centerpoint of the planet disk out to the edges. Integration of expression (10) provides

$$R_{1,2} = D(\omega) \cdot \frac{\sin\left(\pi \frac{B_{r_{1,2}}}{\lambda} \nu\right)}{\pi \frac{B_{r_{1,2}}}{\lambda} \nu} \tag{11}$$

For the situation where the planet appears as a point noise source, the sin x/x type of expression above approaches 1. The brightness transform becomes the total power of the noise source (planet) as seen in the predetection bandwidth, and the preceding discussion relating to a point noise source applies. Figure 18 shows expression (11) plotted as a function of the ratio of planet angular size to fringe spacing $[\nu/(\lambda/B_{r_{1,2}})]$. Note that the above integral is centered ($\nu = 0$) on the in-phase detection noise situation at the center of an angular segment $\lambda/2B_{r_{1,2}}$ that was discussed earlier in this section of the report. Figure 18 is the resultant amplitude of the brightness transform for this particular path length situation to the two antennas for various ratios of planet angular size to fringe spacing. This figure shows the magnitude of the correlated portion of noise power relative to total noise power from the planet, which is defined as fringe visibility for radio interferometry measurements (Ref. 3). Consequently, Fig. 18 provides the information necessary to scale the coherent portion of predetection noise relative to a point noise source for any ratio of planet angular size to fringe spacing $[\nu/(\lambda/B_{r_{1,2}})]$. Any point on Fig. 18 can be treated as an equivalent reduced-in-magnitude point noise source representing a reduced ϵ, and the resulting reduction in predetection signal-to-noise ratio and RF carrier margin improvement can be determined from Figs. 2, 3, 6, 7, 10, 11, 12 and 13.

Consider next three receiving systems (1, 2, and 3) arrayed for coherent reception of a spacecraft signal with a planet within the beamwidth of the three antennas. For the moment, consider a situation where the planet appears as a point noise source which represents a given fractional part ϵ of the operating equivalent system noise temperature T_{op}. At those times when the noise radiation from the planet as seen in the predetection bandwidth of the array is in phase from receivers 1 and 3 in an angular segment $\lambda/2B_{r_{1,3}}$ at essentially the same time as it is from receivers 1 and 2 in an angular segment $\lambda/2B_{r_{1,2}}$, the decrease in predetection signal-to-noise ratio improvement shown in Figs. 4 and 5 applies for the corresponding $(1 - \epsilon)$ value. At all other times, the decrease in predetection signal-to-noise ratio improvement will be less. This discussion also applies to RF carrier margin improvement shown in Figs. 15 and 17 for three systems arrayed. Cross plots of the performance shown in Figs. 8 and 9 and in Figs. 14 and 16 would provide similar information for other signal summing voltage couplings.

For the situation where the planet is not a point source, the normalized brightness transforms for three receiving systems become

$$R_{1,2,3} = \frac{D(\omega)}{2}\left(\frac{\sin\left(\pi \frac{B_{r_{1,2}}}{\lambda}\nu\right)}{\pi \frac{B_{r_{1,2}}}{\lambda}\nu} + \frac{\sin\left(\pi \frac{B_{r_{1,3}}}{\lambda}\nu\right)}{\pi \frac{B_{r_{1,3}}}{\lambda}\nu}\right) \tag{12}$$

Note again in this case that the above expression (12) represents a result centered ($\nu = 0$) on the in-phase predetection noise situation at the center of angular segment $\lambda/2B_{r1,2}$ and simultaneously at the center of angular segment $\lambda/2B_{r1,3}$. For this particular path length situation and given fringe spacings $\lambda/B_{r1,2}$ and $\lambda/B_{r1,3}$, expression (12) can be evaluated and the effect of the planet on decrease in predetection signal-to-noise ratio and RF carrier margin improvement can be determined from Figs. 4, 5, 8, 9, 14, 15, 16, and 17.

In order to illustrate the effect of a planet in the solar system on signal-to-noise ratio improvement for an array of receiving systems as described in Sections II and III of this report, consider reception at 8420 MHz ($\lambda = 3.56$ cm). Table 2 shows nominal radio disk temperatures T_R of the planets in the solar system at a reception wavelength of 3.55 to 3.6 cm, angular size as seen from Earth, and increase in system noise temperature due to the planet in the antenna beamwidth of the 64-meter-diameter antenna. References 4, 5, 6, 7, and 8 provide the basis for the information shown in Table 2. Increase in system noise temperature ΔT_A due to a planet in the antenna beamwidth is obtained (except for Jupiter, due to its radiation belts) from the expression

$$\Delta T_A = T_R \times \frac{\text{planet (source) solid angle}}{\text{antenna beam solid angle}}$$

where the antenna beam solid angle is calculated from the expression (4/3)(half-power beamwidth)^2 (Ref. 4). Increase in system noise temperature due to Jupiter is obtained from the normalized flux density at 4.04 AU using the expression

$$\Delta T_A = \frac{\text{Antenna Geometrical Area} \times \text{Aperture Efficiency} \times \text{Flux Density}}{2 \times (\text{Boltzmann's constant})}$$

and scaling ΔT_A for minimum and maximum distance from Earth by (ratio of distances)^2 (Ref. 8). It is interesting to note that ΔT_A for the outer planets Saturn, Uranus, and Neptune can also be obtained from their normalized flux densities (as with Jupiter), utilizing the information in Ref. 8. The ΔT_A for these three planets obtained by this method essentially agree with the ΔT_A obtained by using T_R and solid angles as described above. It should be noted that expressions (11) and (12) above assume that the planet disk has a uniform brightness distribution $D(w)$ at the reception frequency. Nonthermal radio emission from Jupiter's radiation belts contributes to Jupiter's brightness temperature at a wavelength of 3.56 cm (Refs. 5 and 6), and in addition, the brightness temperature changes with time at this wavelength. Consequently, the above assumption of uniform

brightness distribution is not strictly true for Jupiter and a small error results. Note that the planets Jupiter and Venus produce the largest increase in system noise temperature.

Consider two receiving systems (a 64- and 34-meter-diameter antenna) arrayed for reception of a spacecraft signal. A planet is within the beamwidth of the antennas. The following set of components of antenna feed spacing perpendicular to the line of sight to the planet ($B_{r_{1,2}}$) provides a corresponding set of fringe spacings ($\lambda/B_{r_{1,2}}$) as shown below

$B_{r_{1,2}}$, meters	Fringe spacing ($\lambda/B_{r_{1,2}}$), arc sec
100	73.50
200	36.75
300	24.50
400	18.37
500	14.70

Consider a situation where a $B_{r_{1,2}}$ of 200 meters represents operation of a 64-meter-diameter antenna receiving system (system 1) at an antenna elevation angle of about 60 deg (fringe spacing is 36.75 arcsec). The system noise temperature is 20 + 1 or 21 kelvins (excluding noise contribution from a planet). The planet Jupiter is in the beamwidth of each of the two antennas. Jupiter is at closest approach to the Earth so that it subtends an angle of 50 arcsec and its contribution to the system noise temperature of the 64-meter-diameter antenna receiving system is 13 kelvins (Table 2). The ratio of 50/36.75 equals 1.36 which, from Fig. 18, provides a reduction in relative magnitude of correlated noise power from one to 0.21, which represents 2.7 kelvins. The operating system noise temperature (system 1) is 21 + 13 or 34 kelvins. The statistically independent portion ($1 - \epsilon_1$) of predetection noise power is (34 - 2.7)/34 or 0.92 for system 1. For an array of two receiving systems utilizing a 34-meter-diameter transmit/receive antenna in conjunction with a 64-meter-diameter antenna (Fig. 3), the improvement in predetection signal-to-noise ratio is reduced from 1.0 dB for $1 - \epsilon_1 = 1.0$ to 0.91 dB for $1 - \epsilon_1 = 0.92$ or 0.09 dB ($\gamma_2 = 0.53$). The reduction in RF carrier margin improvement (Fig. 13) is also 0.09 dB. This 0.09-dB reduction in array performance at $1 - \epsilon_1 = 0.92$ essentially applies over the range of γ_2 values shown in Figs. 3 and 13 and also to Figs. 7 and 12 over a large portion of the voltage coupling (β_2) range shown. Note that, in light of the discussion above relative to expressions (10) and (11), this 0.09-dB reduction applies at those times when the path length to the two antennas represents an in-phase predetection noise situation (2.7 kelvins) due to the planet Jupiter. At those times when the path lengths represent an out-of-phase predetection noise situation for the 2.7 kelvins, the predetection signal-to-noise ratio and carrier margin improvement will be larger than the values shown in Figs. 3 and 13 for $1 - \epsilon_1 = 1.0$. The periodic reduction in predetection signal-to-noise ratio and RF carrier margin improvement for the situation discussed above is included as the first array configuration (first line) in Table 3 under the column titled Maximum Periodic Reduction in Array Gain.

Table 3 shows periodic reduction in array gain (as defined in the discussion above) at a reception frequency of 8420 MHz (λ = 3.56 cm) for two receiving systems arrayed (64- and 34-meter-diameter antenna) with the planets Jupiter or Venus in the antenna beamwidth at either minimum or maximum distance from Earth. The table includes a few selected values of $B_{r_{1,2}}$ (component of antenna feed spacing perpendicular to the line of sight to the planet) at antenna elevation angles of approximately 60 and 20 deg. The $B_{r_{1,2}}$ value of 100 meters (shown with an asterisk) is not representative of planned antenna spacings for the DSN. It is included to illustrate the effect on array gain reduction due to the planets for closer antenna feed spacings. The planets Jupiter and Venus were chosen since their presence in the antenna beamwidth produces the largest effect on periodic array gain reduction.

The calculated performance shown in Table 3 is expanded in Figs. 19 through 26 to provide a more graphic presentation of the maximum periodic reduction in array gain as a function of $B_{r_{1,2}}$ for Jupiter (Figs. 19, 20, 23, and 24), or for Venus (Figs. 21, 22, 25, and 26)) in the array beamwidth at their minimum and maximum distances from Earth. Planned antenna spacings and orientation relative to the spin axis of the Earth provide a $B_{r_{1,2}}$ in the range from 195 to 290 meters for a 34-meter-diameter

transmit/receive antenna arrayed with a 64-meter-diameter antenna and a $B_{r_{1,2}}$ in the range from 445 to 550 meters for a 34-meter-diameter listen-only antenna arrayed with a 64-meter-diameter antenna.

Note that for a 34-meter transmit/receive and 64-meter-diameter antenna array, a $B_{r_{1,2}}$ in the 195 to 290 meter range results in a maximum periodic reduction in array gain of 0.1 dB or less for Jupiter in the array beamwidth and 0.17 dB or less for Venus in the array beamwidth. For a 34-meter listen-only and 64-meter-diameter antenna array, a $B_{r_{1,2}}$ in the range from 445 to 550 meters results in a maximum periodic reduction in array gain of 0.05 dB or less for Jupiter in the array beamwidth and 0.1 dB or less for Venus in the array beamwidth.

Table 4 shows periodic reduction in array gain at a reception frequency of 8420 MHz for an array of three receiving systems with the planets Jupiter or Venus in the antenna beamwidth as in Table 3. The array utilizes a 64-meter-diameter antenna (system 1), a 34-meter-diameter listen-only antenna (system 2) and a 34-meter-diameter transmit/receive antenna (system 3) with antenna feed spacings (component perpendicular to the line of sight to the planet) of 500 meters ($B_{r_{1,2}}$) and 200 meters ($B_{r_{1,3}}$). This is representative of the planned three station array in Australia at an elevation angle of approximately 50 deg.

It should be noted that with the planets Uranus or Neptune in the antenna beamwidth (see Table 2) their effect on array gain is negligible even though (for the planned antenna feed spacings discussed above) most of the noise contribution from Uranus or Neptune will be coherent periodically.

References

1. Brockman, M. H., "The Effect of Partial Coherence in Receiving System Noise Temperature on Array Gain for Telemetry and Radio Frequency Carrier Reception for Similar Receiving Systems," in *TDA Progress Report 42-66*, pp. 219-235, Jet Propulsion Laboratory, Pasadena, Calif., Dec. 15, 1981.
2. Divsalar, D., and Yuen, J. H., "Improved Carrier Tracking Performance with Coupled Phase-Locked Loops," in *TDA Progress Report 42-66*, pp. 148-171, Jet Propulsion Laboratory, Pasadena, Calif., Dec. 15, 1981.
3. Thomas, J. B., *An Analysis of Source Structure Effects in Radio Interferometry Measurements*, Publication 80-84, Jet Propulsion Laboratory, Pasadena, Calif., Dec. 15, 1980.
4. Kraus, J. D., *Radio Astronomy*, McGraw-Hill Book Company, New York, 1966.
5. Newburn, R. L., Jr., and Gulkis, S., "A Survey of the Outer Planets Jupiter, Saturn, Uranus, Neptune, Pluto, and Their Satellites," *Space Science Reviews*, 3, pp. 179-271, 1973.
6. Gulkis, S., "Thermal Radio Emissions from the Major Planets," *Space Science Reviews*, 14, pp. 497-510, 1973.
7. Allen, C. W., *Astrophysical Quantities*, 3rd ed., University of London, The Athlone Press, London, 1973.
8. Turegano, J. A., and Klein, M. J., "Precision Flux Density Measurements of the Giant Planets at 8420 MHz," *Astronomy & Astrophysics*, 94, pp. 91-94, 1981.

Table 1. RF carrier array gain measurements

($\gamma_2 = \gamma_3 = 0.61; N_{o2}/N_{o1} = N_{o3}/N_{o1} = 1$ for $1 - \epsilon_1 = 1$)

Two receiving systems				Three receiving systems			
		Array gain, dB				Array gain, dB	
$1 - \epsilon_1$	β_2	Theory	Measured	$1 - \epsilon_1$	$\beta_2 = \beta_3$	Theory	Measured
1.0	0.5	1.3	1.3	1.0	1.0	1.9	1.8
1.0	0.43	1.23	1.2	1.0	0.97	1.94	1.9
0.73	0.5	0.92	0.9	1.0	0.61	2.28	2.3
0.73	0.43	0.88	0.8	0.73	1.0	1.33	1.2
0.21	0.5	0.28	0.2	0.73	0.61	1.55	1.6
0.21	0.41	0.24	0.2	0.21	0.59	0.46	0.4

Table 2. Increase in system noise temperature due to the planets; 64-meter-diameter antenna; λ = 3.55 to 3.6 km

Planet	Nominal radio disk temperature (T_R), K	Subtended angle from earth, arcsec		Increase in system noise temperature, K	
		max.	min.	max.	min.
Mercury	330	13	5	1.8	0.3
Venus	600	67	17	85.0	5.5
Mars	200	24	4	3.6	0.1
Jupiter	230	50	32	13.0	5.0
Saturn	165	20	14	1.4	0.7
Uranus	210	3.6		0.08	
Neptune	200	2.2		0.03	

Table 3. Maximum periodic reduction in array gain due to a planet within beamwidth of two-aperture array (two receiving systems arrayed for coherent reception; reception frequency 8420 MHz; $\lambda = 3.56$ cm)

Array configuration	Antenna elevation angle, deg	Planet in array beamwidth	Planet subtended angle from earth ν, arcsec	$B_{r1,2}$ m	$\nu/\left(\frac{\lambda}{B_{r1,2}}\right)$	Maximum periodic reduction in array gain, dB
64- and 34-m transmit/receive	~60	Jupiter	50	200	1.36	0.09
	~20		50	200	1.36	0.07
	~60		32	200	0.87	0.04
	~20		32	200	0.87	0.03
	~60		50	100[a]	0.68	0.18
	~20		50	100[a]	0.68	0.14
	~60		32	100[a]	0.44	0.16
	~20		32	100[a]	0.44	0.12
	~60	Venus	67	200	1.82	0.09
	~20		67	200	1.82	0.08
	~60		17	200	0.46	0.16
	~20		17	200	0.46	0.12
	~60		67	100[a]	0.91	0.09
	~20		67	100[a]	0.91	0.08
	~60		17	100[a]	0.23	0.22
	~20		17	100[a]	0.23	0.16
64- and 34-m listen-only	~60	Jupiter	50	200	1.36	0.13
	~20		50	200	1.36	0.09
	~60		32	200	0.87	0.05
	~20		32	200	0.87	0.04
	~60		50	500	3.40	0.05
	~20		50	500	3.40	0.04
	~60		32	500	2.18	0.03
	~20		32	500	2.18	0.02
	~60	Venus	67	200	1.82	0.13
	~20		67	200	1.82	0.11
	~60		17	200	0.46	0.22
	~20		17	200	0.46	0.15
	~60		67	500	4.56	0.09
	~20		67	500	4.56	0.08
	~60		17	500	1.16	0.04
	~20		17	500	1.16	0.03

[a]Not planned for the DSN.

Table 4. Maximum periodic reduction in array gain due to a planet within beamwidth of three-aperture array (three receiving systems arrayed for coherent reception; reception frequency 8420 MHz; λ = 3.56 cm)

Array configuration	Antenna elevation angle, deg	Planet in array beamwidth	Planet subtended angle from earth ν, arc sec	$B_{r1,2}$, m	$\nu/\left(\frac{\lambda}{B_{r_{1,2}}}\right)$	$B_{r1,3}$, m	$\nu/\left(\frac{\lambda}{B_{r_{1,3}}}\right)$	Maximum periodic reduction in array gain, dB
64- and 34-m listen-only and 34-m transmit/ receive	~60	Jupiter	50	500	3.40	200	1.36	0.15
	~20		50	500	3.40	200	1.36	0.12
	~60		32	500	2.18	200	0.87	0.06
	~20		32	500	2.18	200	0.87	0.04
	~60	Venus	67	500	4.56	200	1.83	0.18
	~20		67	500	4.56	200	1.83	0.17
	~60		17	500	1.16	200	0.46	0.23
	~20		17	500	1.16	200	0.46	0.17

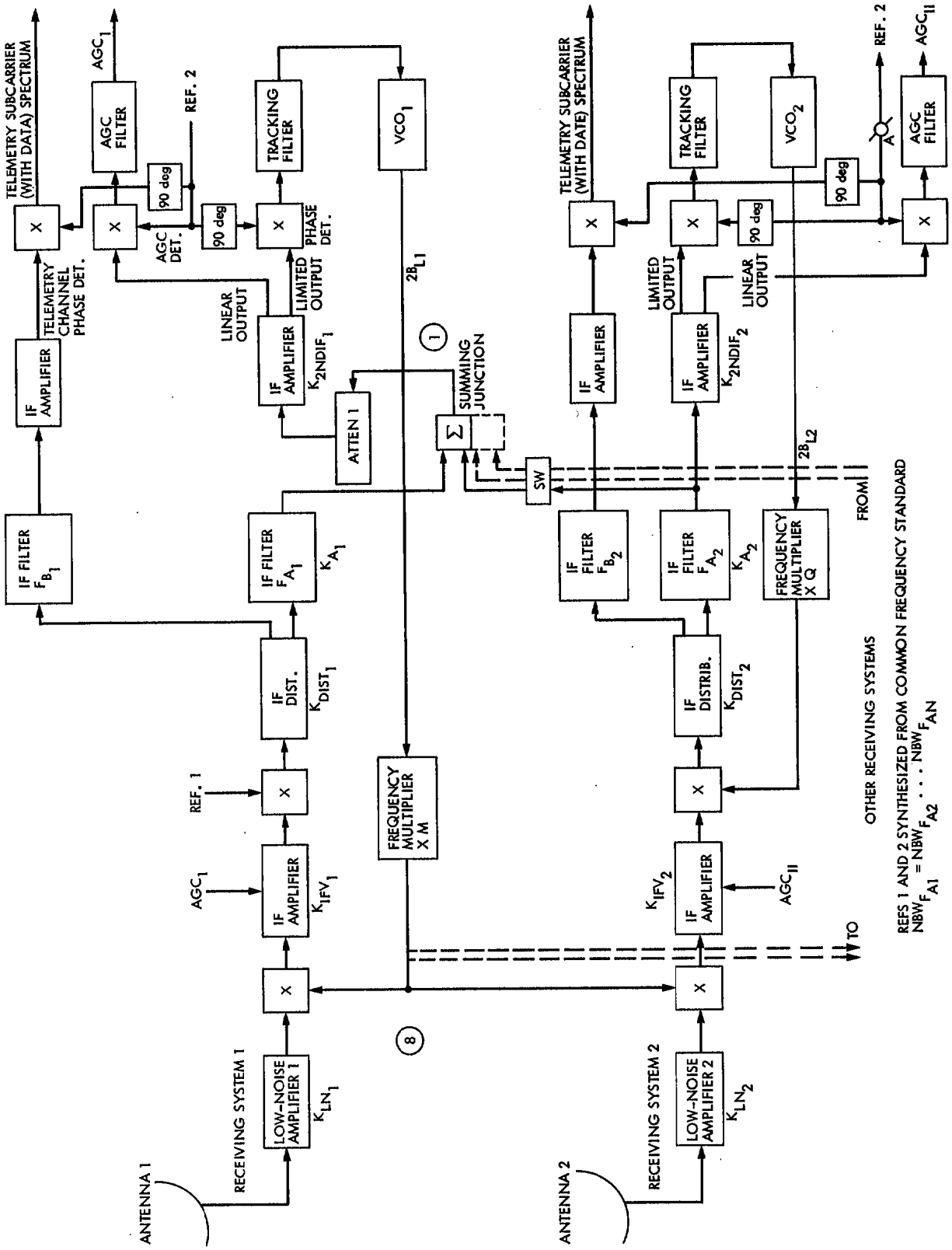

Fig. 1. Radio frequency carrier arraying for high-rate telemetry reception

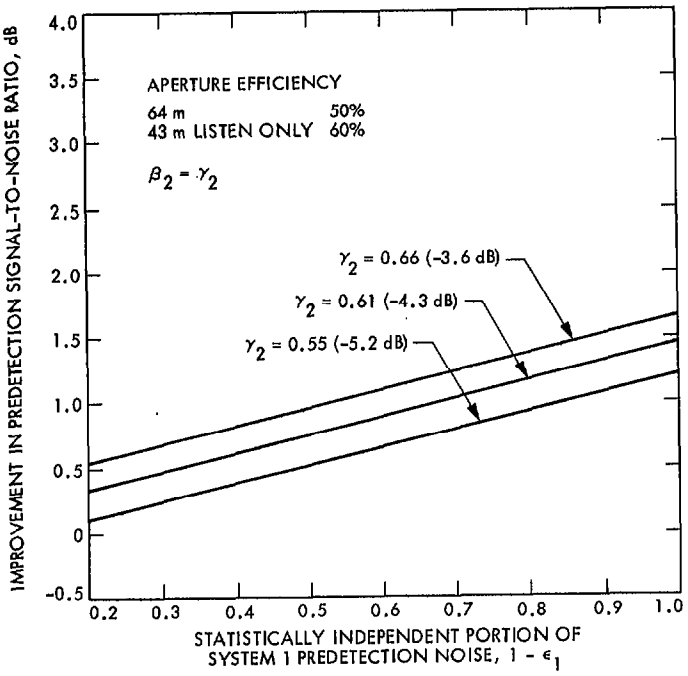

Fig. 2. Effect of partial coherence in system noise temperature on predetection signal-to-noise ratio improvement, two receiving systems arrayed, 64- and 34-m-diameter listen-only antennas

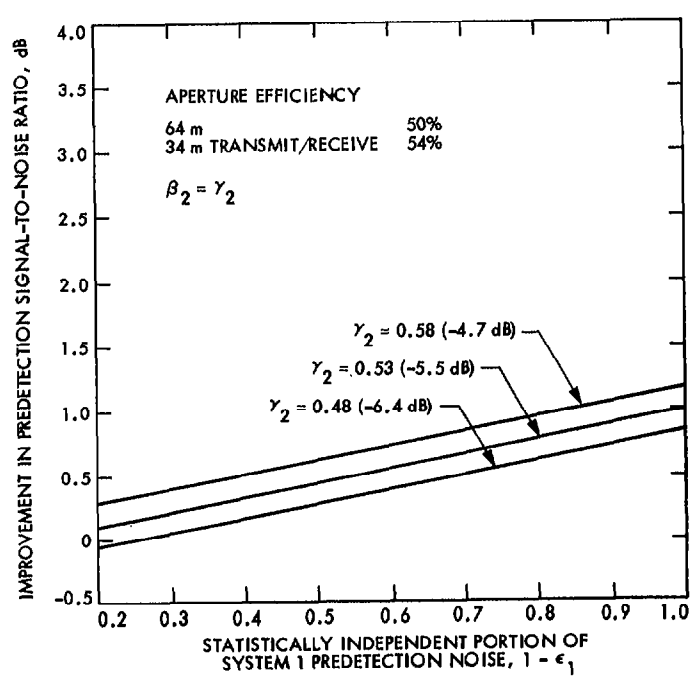

Fig. 3. Effect of partial coherence in system noise temperature on predetection signal-to-noise ratio improvement, two receiving systems arrayed, 64- and 34-m-diameter transmit/receive antennas

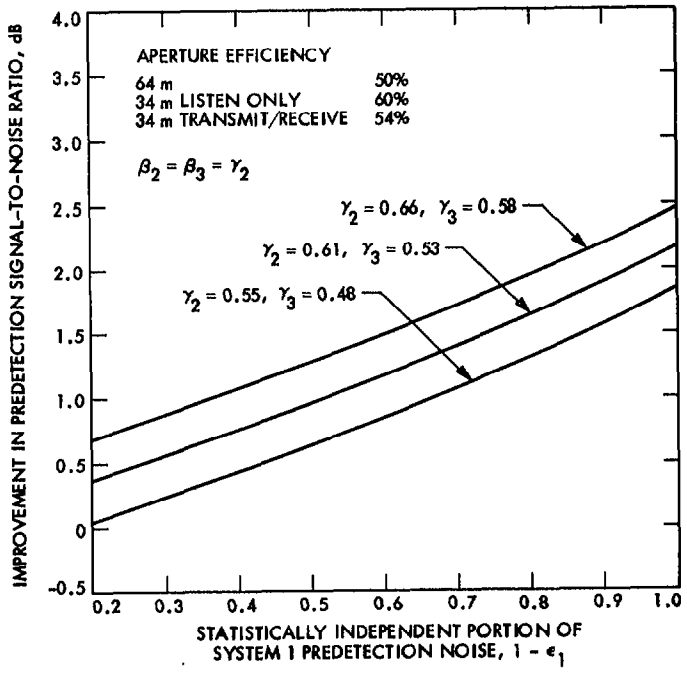

Fig. 4. Effect of partial coherence in system noise temperature on predetection signal-to-noise ratio improvement, three receiving systems arrayed; 64- and 34-m-diameter listen-only and 34-m-diameter transmit/receive antennas

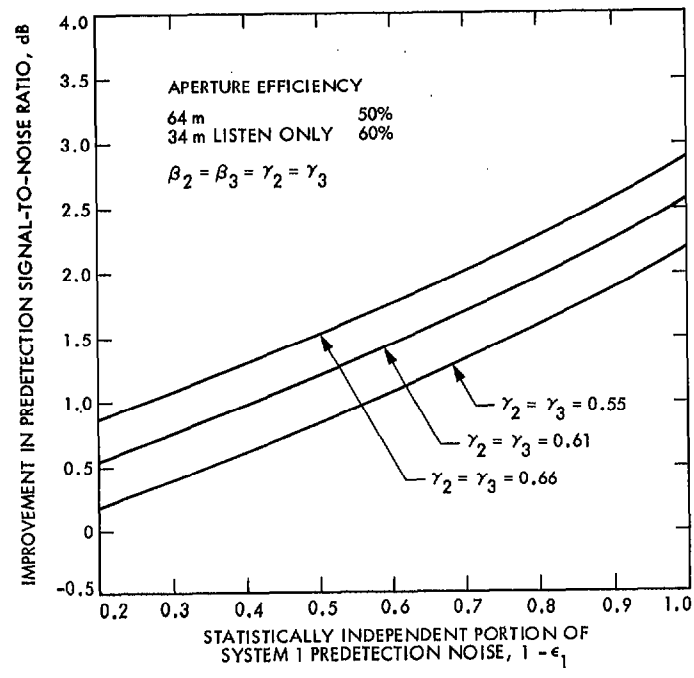

Fig. 5. Effect of partial coherence in system noise temperature on predetection signal-to-noise ratio improvement, three receiving systems arrayed, 64-m-diameter and two 34-m-diameter listen-only antennas

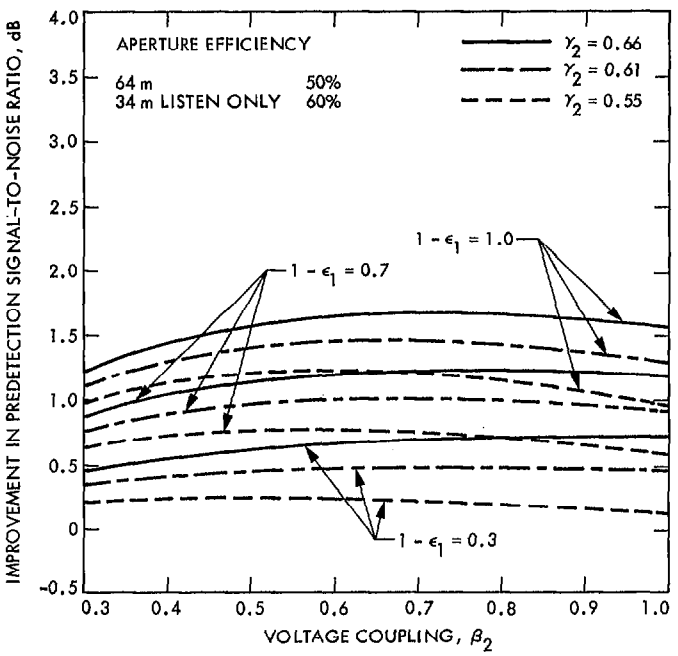

Fig. 6. Effect of signal summing voltage coupling on predetection signal-to-noise ratio improvement with partial coherence in system noise temperature, two receiving systems arrayed, 64- and 34-m-diameter listen-only antennas

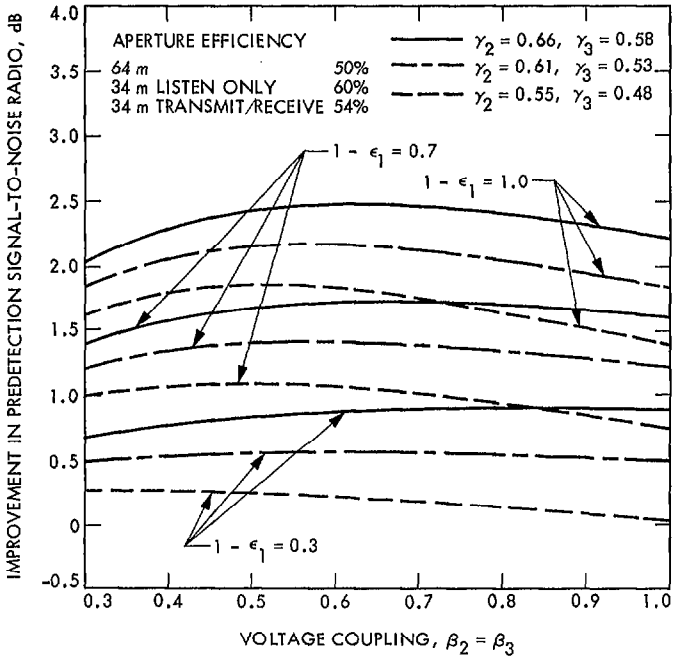

Fig. 8. Effect of signal summing voltage coupling on predetection signal-to-noise ratio improvement with partial coherence in system noise temperature, three receiving systems arrayed; 64-m-diameter, 34-m-diameter listen only, and 34-m-diameter transmit/receive antennas

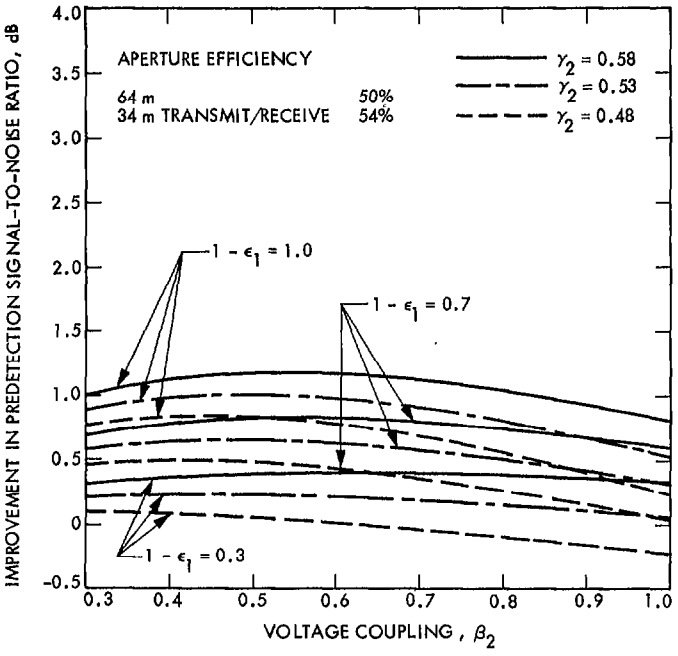

Fig. 7. Effect of signal summing voltage coupling on predetection signal-to-noise ratio improvement with partial coherence in system noise temperature, two receiving systems arrayed, 64- and 34-m-diameter transmit/receive antennas

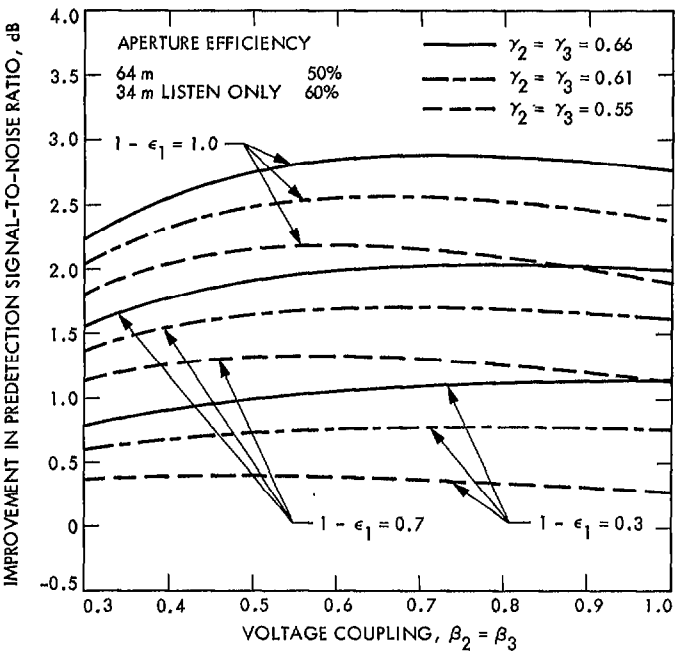

Fig. 9. Effect of signal summing voltage coupling on predetection signal-to-noise ratio improvement with partial coherence in system noise temperature, three receiving systems arrayed; 64-m-diameter and two 34-m-diameter listen-only antennas

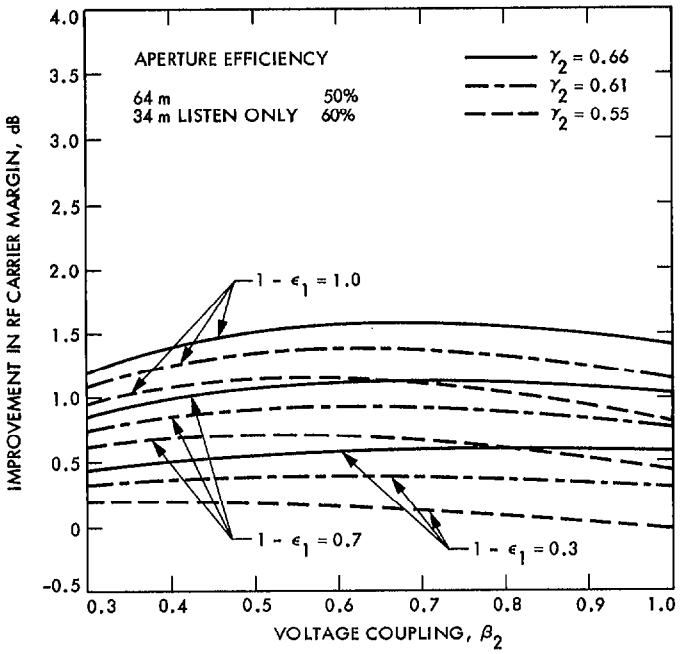

Fig. 10. Effect of summing junction voltage coupling on RF carrier margin improvement with partial coherence in system noise temperature, two receiving systems arrayed, 64- and 34-m-diameter listen-only antennas

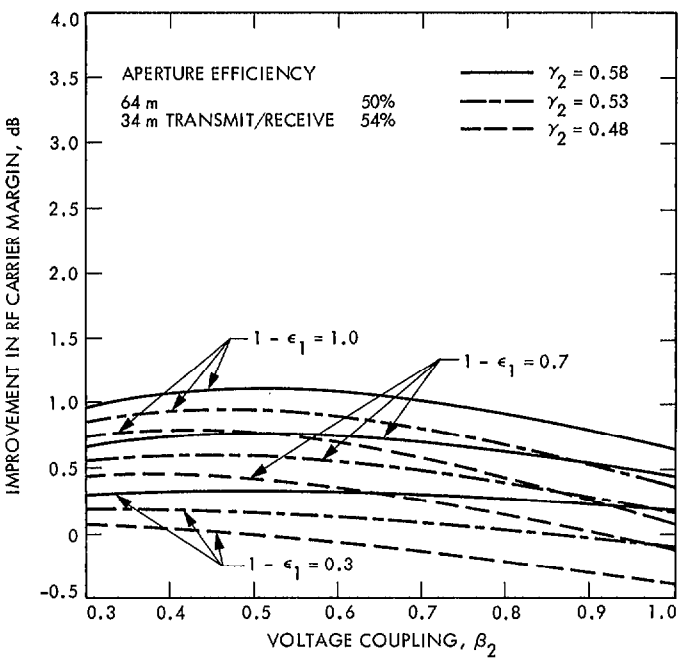

Fig. 12. Effect of summing junction voltage coupling on RF carrier margin improvement with partial coherence in system noise temperature, two receiving systems arrayed, 64- and 34-m-diameter transmit/receive antennas

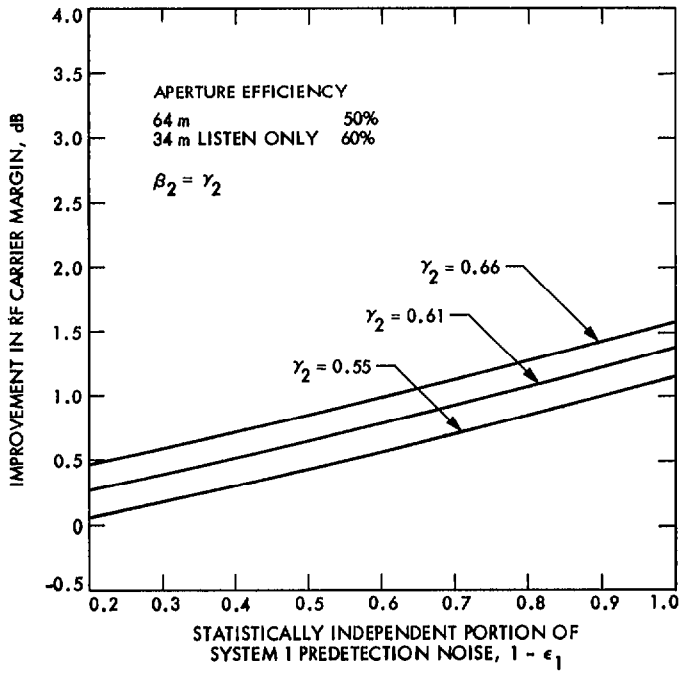

Fig. 11. Effect of partial coherence in system noise temperature on RF carrier margin improvement, two receiving systems arrayed, 64- and 34-m-diameter listen-only antennas

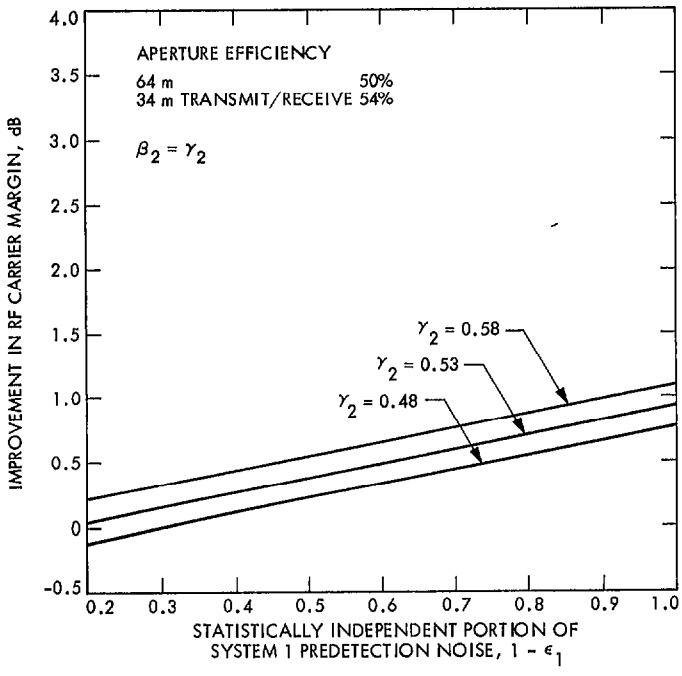

Fig. 13. Effect of partial coherence in system noise temperature on RF carrier margin improvement, two receiving systems arrayed, 64- and 34-m-diameter transmit/receive antennas

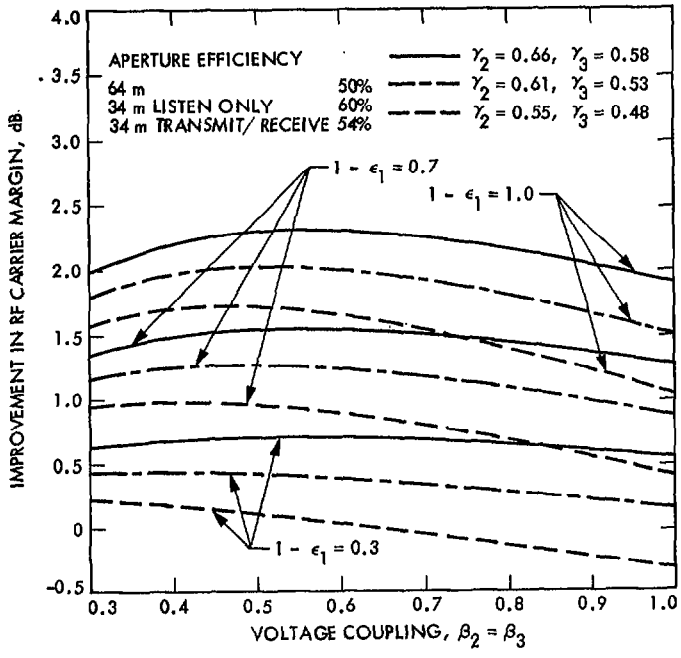

Fig. 14. Effect of summing junction voltage coupling on RF carrier margin improvement with partial coherence in system noise temperature, three receiving systems arrayed; 64-m-diameter, 34-m-diameter listen-only, and 34-m-diameter transmit/receive antennas

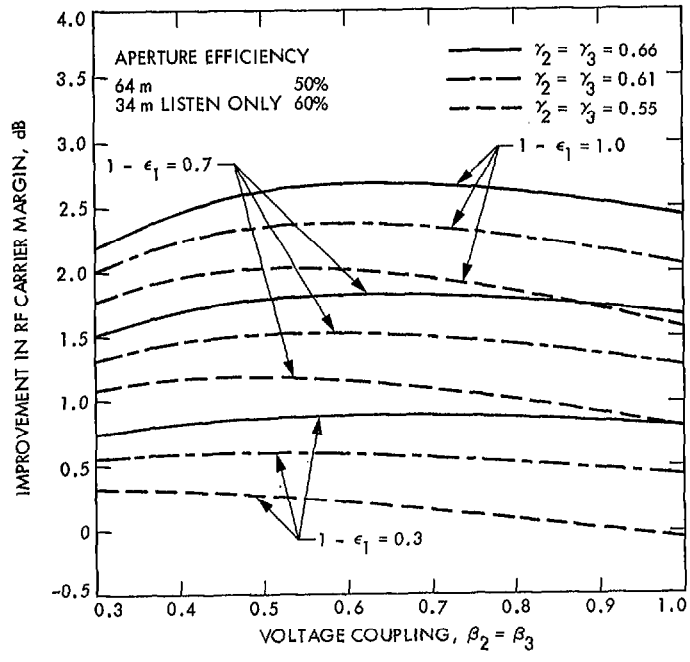

Fig. 16. Effect of summing junction voltage coupling on RF carrier margin improvement, with partial coherence in system noise temperature, three receiving systems arrayed; 64-m-diameter and two 34-m-diameter listen-only antennas

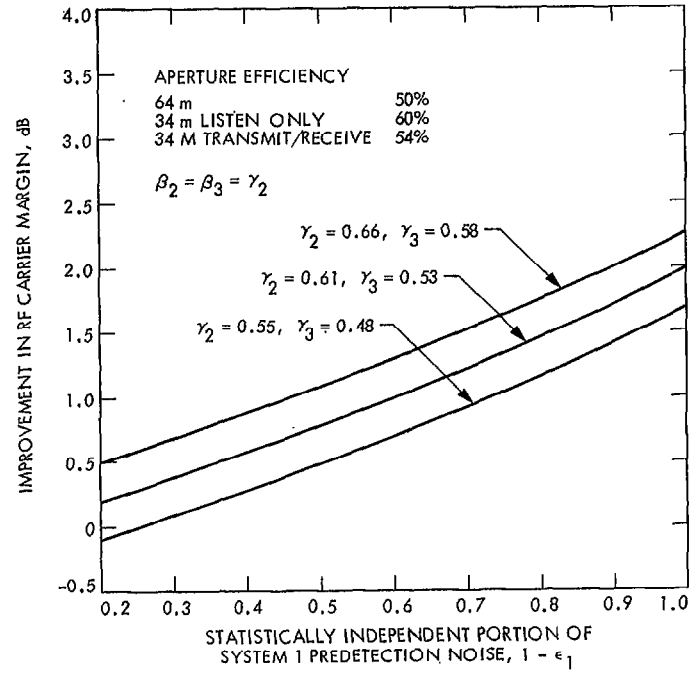

Fig. 15. Effect of partial coherence in system noise temperature on RF carrier margin improvement, three receiving systems arrayed; 64-m-diameter, 34-m-diameter listen-only, and 34-m-diameter transmit/receive antennas

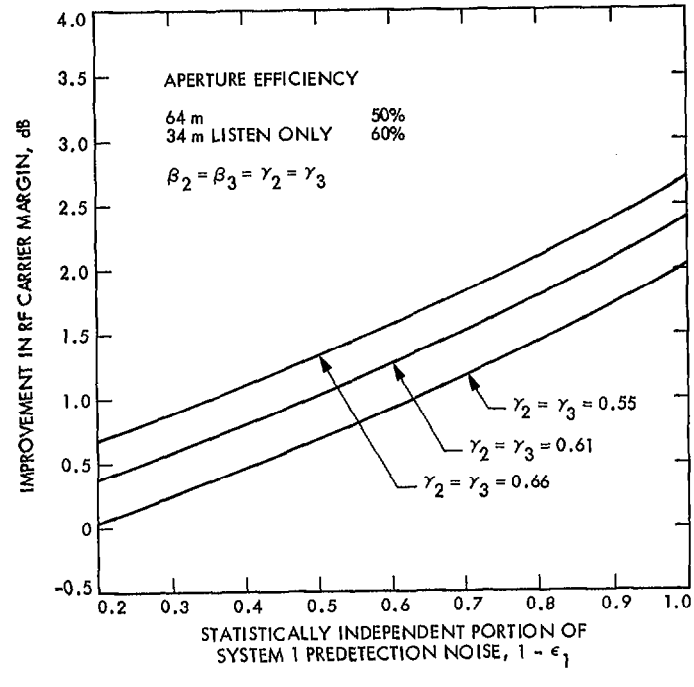

Fig. 17. Effect of partial coherence in system noise temperature on RF carrier margin improvement, three receiving systems arrayed; 64-m-diameter and two 34-m-diameter listen-only antennas

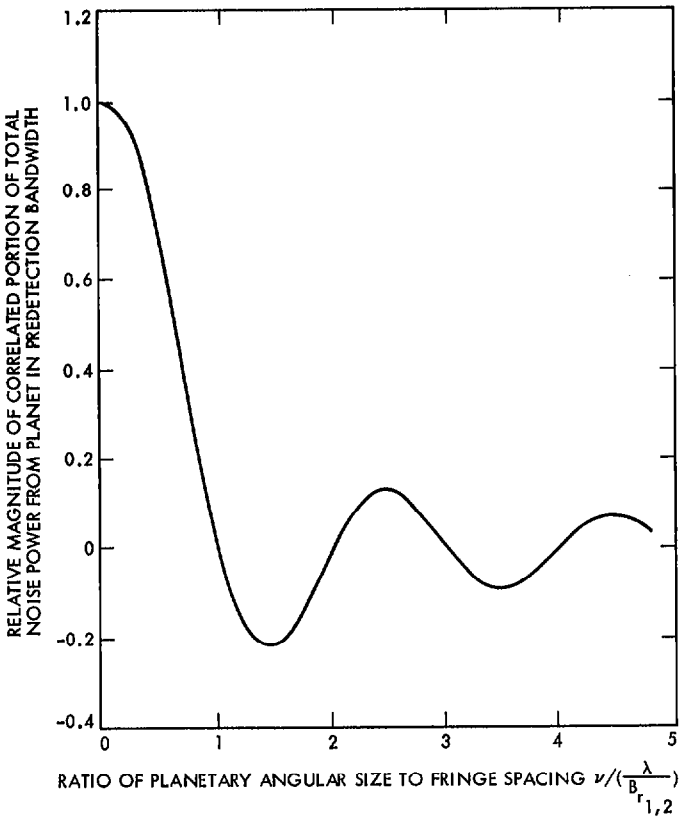

Fig. 18. Relative effect of ratio of planet angular size to fringe spacing on correlated predetection noise, two-antenna array

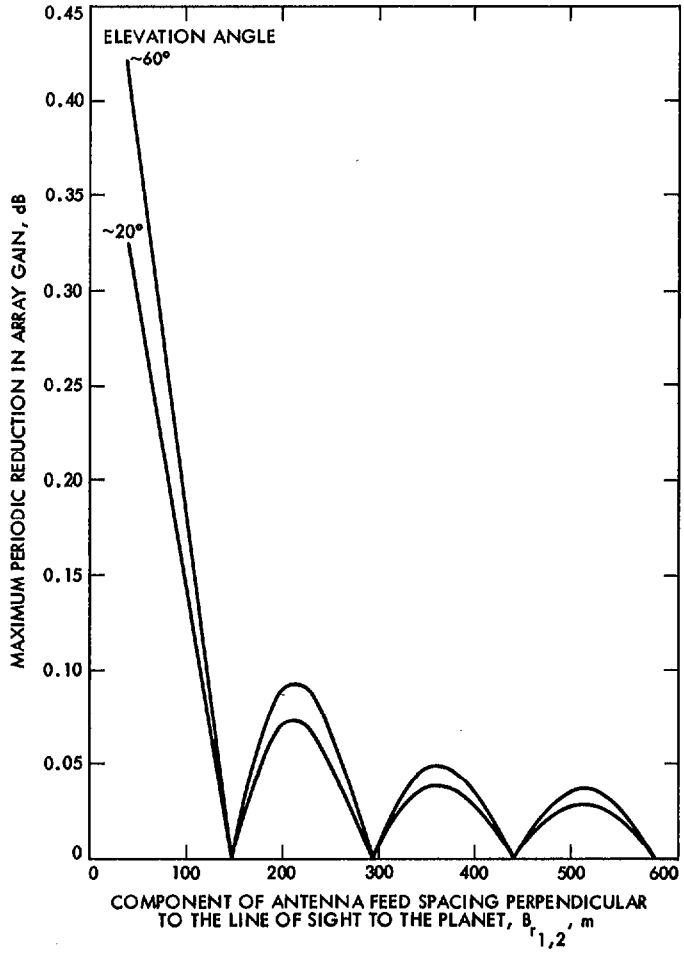

Fig. 19. Maximum periodic reduction in array gain due to Jupiter (at minimum distance) within beamwidth of two receiving systems arrayed for coherent reception vs effective feed spacing; 64- and 34-m-diameter (transmit/receive) antennas, reception at 8420 MHz

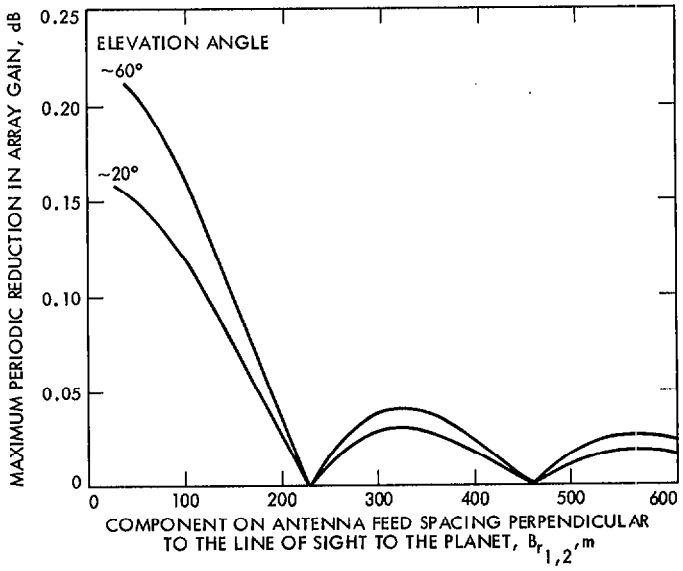

Fig. 20. Maximum periodic reduction in array gain due to Jupiter (at maximum distance) within beamwidth of two receiving systems arrayed for coherent reception vs effective feed spacing; 64- and 34-m-diameter (transmit/receive) antennas, reception at 8420 MHz

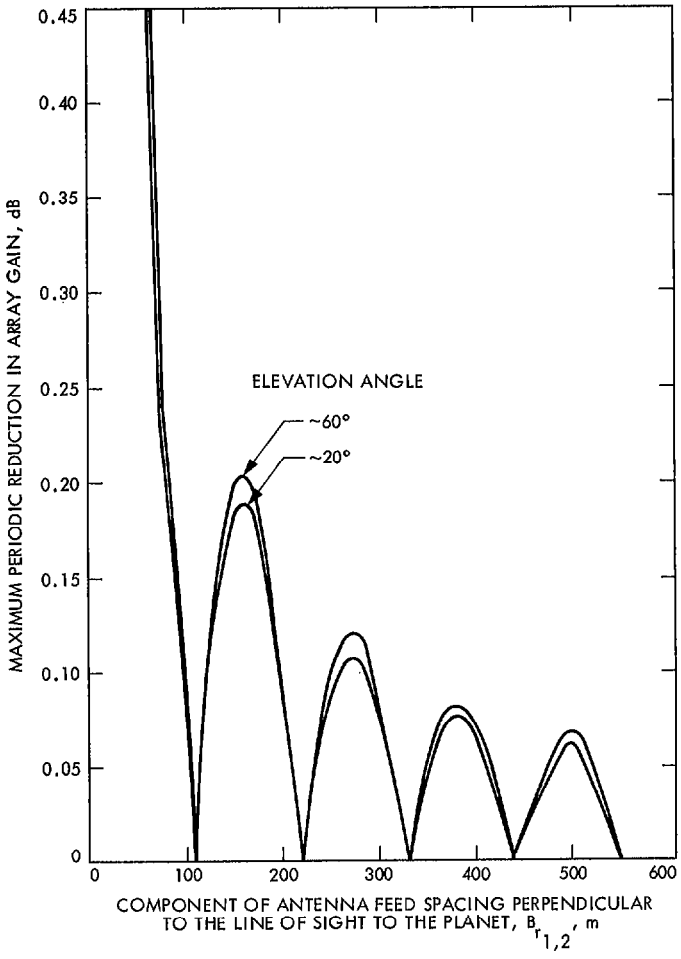

Fig. 21. Maximum periodic reduction in array gain due to Venus (at minimum distance) within beamwidth of two receiving systems arrayed for coherent reception vs effective feed spacing; 64- and 34-m-diameter (transmit/receive) antennas, reception at 8420 MHz

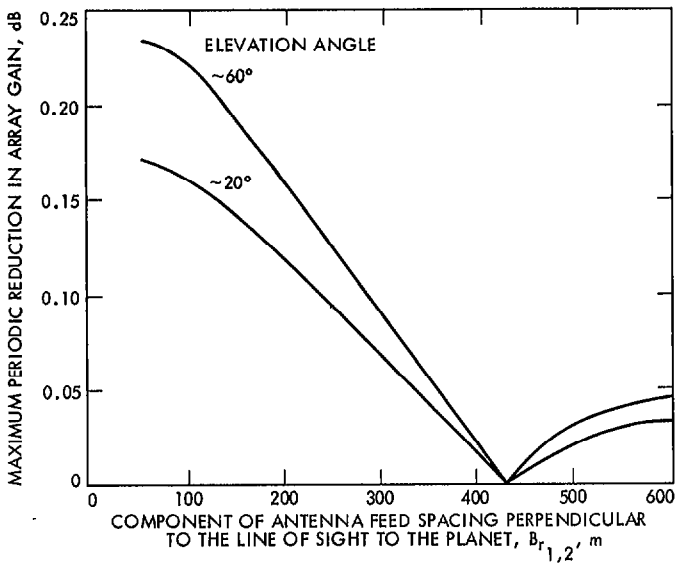

Fig. 22. Maximum periodic reduction in array gain due to Venus (at maximum distance) within beamwidth of two receiving systems arrayed for coherent reception vs effective feed spacing; 64- and 34-m-diameter (transmit/receive) antennas, reception at 8420 MHz

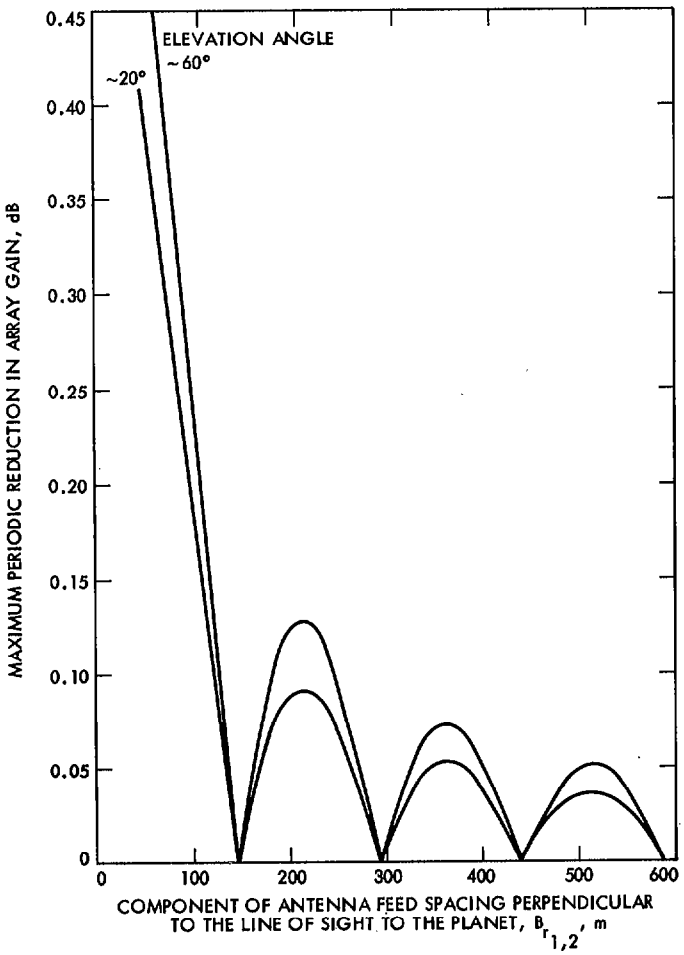

Fig. 23. Maximum periodic reduction in array gain due to Jupiter (at minimum distance) within beamwidth of two receiving systems arrayed for coherent reception vs effective feed spacing; 64- and 34-m-diameter (listen-only) antennas, reception at 8420 MHz

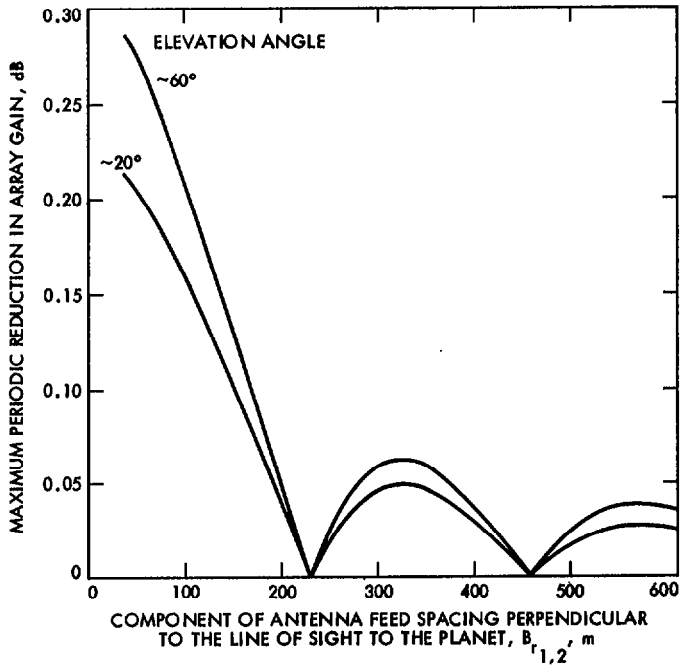

Fig. 24. Maximum periodic reduction in array gain due to Jupiter (at maximum distance) within beamwidth of two receiving systems arrayed for coherent reception vs effective feed spacing; 64- and 34-m-diameter (listen-only) antennas, reception at 8420 MHz

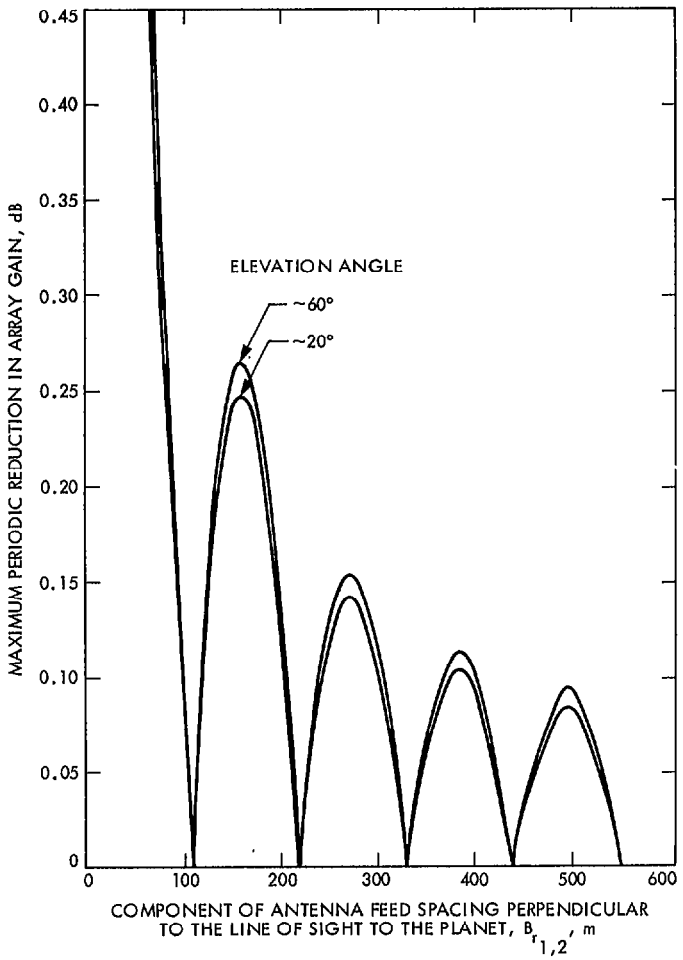

Fig. 25. Maximum periodic reduction in array gain due to Venus (at minimum distance) within beamwidth of two receiving systems arrayed for coherent reception vs effective feed spacing; 64- and 34-m-diameter (listen-only) antennas, reception at 8420 MHz

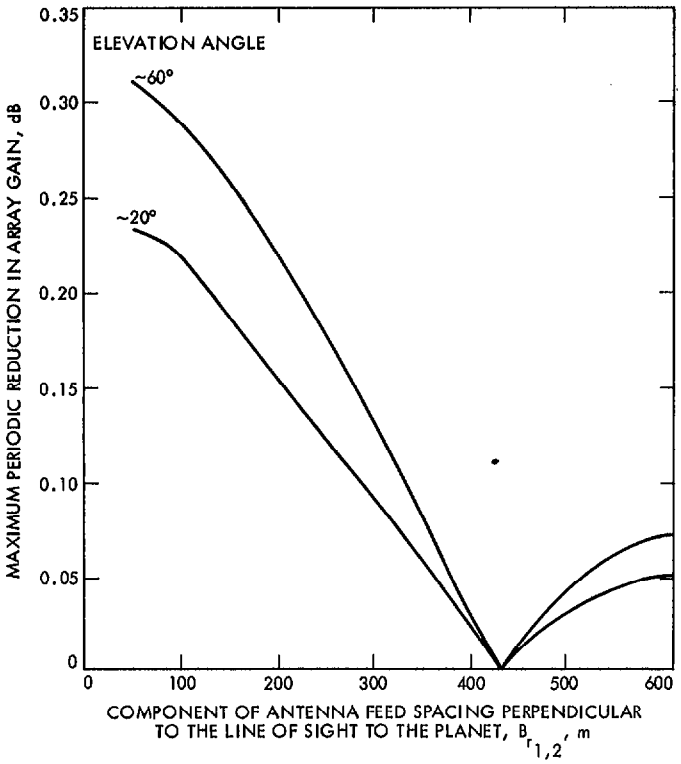

Fig. 26. Maximum periodic reduction in array gain due to Venus (at maximum distance) within beamwidth of two receiving systems arrayed for coherent reception vs effective feed spacing; 64-and 34-m-diameter (listen-only) antennas, reception at 8420 MHz